nature protocols

https://doi.org/10.1038/s41596-024-01085-w

Protocol

Check for updates

Versatile MRI acquisition and processing protocol for population-based neuroimaging

Alexandra Koch[1], Rüdiger Stirnberg[2], Santiago Estrada[1,3], Weiyi Zeng[1], Valerie Lohner[1], Mohammad Shahid[1], Philipp Ehses[2], Eberhard D. Pracht[2], Martin Reuter[3,4,5] ✉, Tony Stöcker[2,6] ✉ & Monique M. B. Breteler[1,7] ✉

Abstract

Neuroimaging has an essential role in studies of brain health and of cerebrovascular and neurodegenerative diseases, requiring the availability of versatile magnetic resonance imaging (MRI) acquisition and processing protocols. We designed and developed a multipurpose high-resolution MRI protocol for large-scale and long-term population neuroimaging studies that includes structural, diffusion-weighted and functional MRI modalities. This modular protocol takes almost 1 h of scan time and is, apart from a concluding abdominal scan, entirely dedicated to the brain. The protocol links the acquisition of an extensive set of MRI contrasts directly to the corresponding fully automated data processing pipelines and to the required quality assurance of the MRI data and of the image-derived phenotypes. Since its successful implementation in the population-based Rhineland Study (ongoing, currently more than 11,000 participants, target participant number of 20,000), the proposed MRI protocol has proved suitable for epidemiological and clinical cross-sectional and longitudinal studies, including multisite studies. The approach requires expertise in magnetic resonance image acquisition, in computer science for the data management and the execution of processing pipelines, and in brain anatomy for the quality assessment of the MRI data. The protocol takes ~1 h of MRI acquisition and ~20 h of data processing to complete for a single dataset, but parallelization over multiple datasets using high-performance computing resources reduces the processing time. By making the protocol, MRI sequences and pipelines available, we aim to contribute to better comparability, interoperability and reusability of large-scale neuroimaging data.

Key points

- This protocol links the acquisition of MRI datasets to their corresponding fully automated data processing pipelines and to the required quality control checks for both the MRI data and the image-derived phenotypes. The approach is suitable for epidemiological and clinical cross-sectional and longitudinal studies, including multisite studies.
- The modular protocol comprises time-efficient high-resolution MRI acquisition and processing and facilitates the comparability, interoperability and reusability of large-scale neuroimaging data.

Key references

Stirnberg, R. et al. *Magn. Reson. Med.* 92, 2294-2311 (2024): https://doi.org/10.1002/mrm.30216

Henschel, L., Kügler, D. & Reuter, M. *NeuroImage* **251**, 118933–118933 (2022): https://doi.org/10.1016/j.neuroimage.2022.118933

Estrada, S. et al. *Mag. Reson. Med.* **83**, 1471–1483 (2020): https://doi.org/10.1002/mrm.28022

[1]Population Health Sciences, German Center for Neurodegenerative Diseases (DZNE), Bonn, Germany. [2]MR Physics, German Center for Neurodegenerative Diseases (DZNE), Bonn, Germany. [3]AI in Medical Imaging, German Center for Neurodegenerative Diseases (DZNE), Bonn, Germany. [4]A.A. Martinos Center for Biomedical Imaging, Massachusetts General Hospital, Boston, MA, USA. [5]Department of Radiology, Harvard Medical School, Boston, MA, USA. [6]Department for Physics and Astronomy, University of Bonn, Bonn, Germany. [7]Institute for Medical Biometry, Informatics and Epidemiology (IMBIE), Faculty of Medicine, University of Bonn, Bonn, Germany. ✉e-mail: Martin.Reuter@dzne.de; Tony.Stoecker@dzne.de; Monique.Breteler@dzne.de

Protocol

Introduction

Technical advances in magnetic resonance imaging (MRI) and the increased accessibility of clinical magnetic resonance (MR) technology, has positioned neuroimaging as an indispensable diagnostic tool in studies of cerebrovascular and neurodegenerative diseases, as well as those of brain health. In large-scale population-based cohort studies, neuroimaging has an essential role; however, it often requires extensive lead times for the design, development and setup of an elaborate MRI study. By making the MRI acquisition and processing protocol of the population-based Rhineland Study available, we aim to support future epidemiological and clinical cross-sectional and longitudinal MRI studies and improve the comparability, interoperability and reusability of the collected imaging data.

Development of the protocol

The proposed MRI acquisition and processing protocol was designed and developed to meet the requirements for large-scale and long-term population neuroimaging in the Rhineland Study, a prospective community-based cohort study that includes participants aged 30 years and above and is scheduled to run for decades. The MRI acquisition protocol is largely based on in-house developed MRI sequences. With a total scan time below 1 h per participant, it allows the acquisition of multiple neuro MR contrasts at 3 Tesla (3T) with high image quality and resolution, while keeping potential participant discomfort and motion artifacts at manageable levels. A challenge in large-scale long-term research is the trade-off between keeping the longitudinally collected data comparable and keeping them relevant and up to date. We thus selected the scan parameters as forward looking as feasible, i.e., with a short scan time and with whole-brain coverage as well as high isotropic image resolution. To keep the MRI scan protocol as constant as possible, but at the same time adaptive, we separated it into a core imaging protocol with MR contrasts of high relevance that will be acquired for all study participants and a free protocol to accommodate alternative promising and innovative MRI techniques in a smaller subpopulation. The proposed MRI analysis protocol meets the requirements to process large-scale imaging data through fast and fully automated, adaptable and expandable quality assessment (QA) and data analysis pipelines that incorporate established state-of-the-art image analysis tools as well as innovative machine learning methods, ensuring high data quality and reproducibility.

The proposed MRI scan and analysis protocol contains four major components (Fig. 1) presenting the protocol workflow: acquisition, preprocessing, QA and postprocessing of the MRI data. Although separate components of this procedure have previously been published[1–15], the proposed MRI protocol describes all four components of the workflow, in particular the application of the respective methodology, as a complete process.

MRI acquisition

The protocol acquires high-resolution imaging data on a 3T MRI scanner (MAGNETOM Prisma, Siemens Healthineers) equipped with a high-performance whole-body gradient system of 80 mT/m amplitude and 200 T/m/s slew rate and a 64-channel head–neck receive array. Except for a concluding abdominal scan, the protocol focuses on whole-brain acquisitions. The core protocol includes T_1-weighted[1,16] (0.8 mm isotropic image resolution), T_2-weighted (0.8 mm isotropic) and T_2 fluid-attenuated inversion recovery (FLAIR, 1.0 mm isotropic) structural MRI, and diffusion-weighted[14] (1.5 mm isotropic), multi-echo T_2*/susceptibility-weighted[13,15] (0.8 mm isotropic), 10 min resting-state functional[12] (2.4 mm isotropic at 0.57 s temporal resolution) and abdominal Dixon fat/water (2.0 mm × 2.0 mm × 5.0 mm) MRI as depicted in Fig. 1. The acquisition time of the core protocol is 45 min. The most relevant MRI sequence parameters are listed in Table 1. The core protocol is based on customized MR sequences, either developed from scratch or based on vendor implementations, which use volumetric acquisitions that allow for two-dimensional (2D) parallel imaging acceleration with reduced aliasing[17,18] and, if possible, elliptical sampling[19]. The MRI signal is thus acquired more signal-to-noise ratio- (SNR) and time-efficiently than usual (Box 1). Only diffusion MRI (dMRI) as well as the abdominal

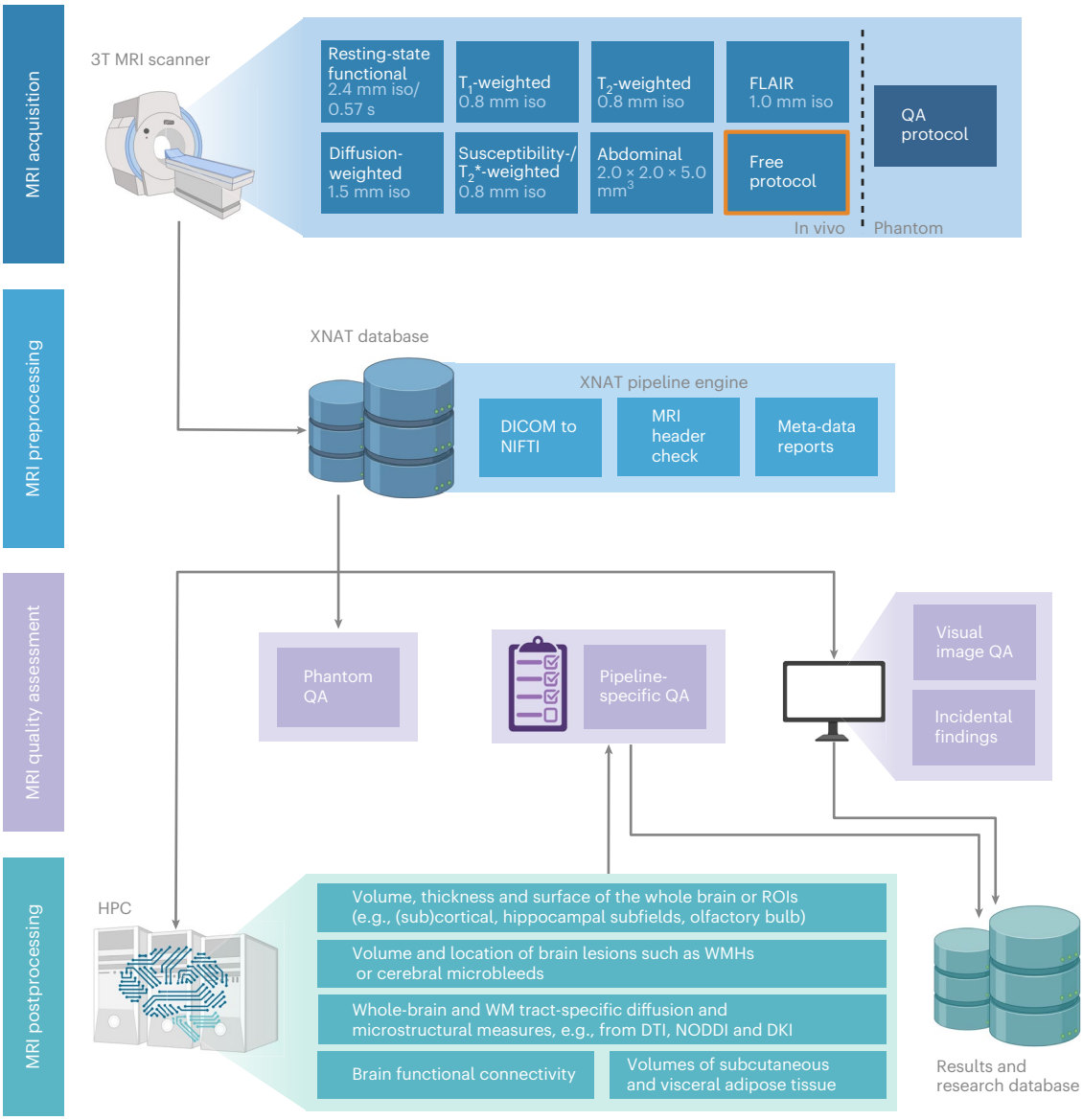

Fig. 1 | Workflow of the MRI acquisition and processing protocol. Protocol described in ref. 7. Acquisition, preprocessing, QA and postprocessing of the MRI data collected in the population-based Rhineland Study. Spatial image resolution is given in units of mm for each MR contrast. Single numbers refer to isotropic (iso) voxel sizes. Only the voxels of the abdominal MRI have unequal side lengths, as specified. ROI, region of interest; DTI, diffusion tensor imaging; DKI, diffusion kurtosis imaging. Figure created with BioRender.com.

scan use unmodified vendor implementations. The resulting gain in scan speed and signal-to-noise ratio allows the acquisition of structural whole-brain contrasts at a comparably high isotropic resolution of 0.8 mm without sacrificing image quality. So far, the free protocol of up to 7 min has been used in the Rhineland Study to perform high-resolution hippocampal subfields imaging, quantitative $T_{1\rho}$ mapping[20] and perfusion imaging[21,22], and is further planned to include chemical exchange saturation transfer[23] MRI and multiparametric mapping[24], where all acquisitions except the first are based on custom sequences. For the free protocol of the proposed MRI protocol, we selected high-resolution hippocampal subfields imaging based on the 2D turbo-spin-echo (TSE) vendor sequence. The free protocol can alternatively be used to run updated MRI sequences in parallel to established sequences to optimize the scan protocol and at the same time to enable the harmonization of MRI data after changes have

Table 1 | The MRI scan protocol of the Rhineland Study acquires many promising MRI contrasts in a short scan time

Contrast	Sequence name	Resolution (mm^3)	PI accel	TA (min)	Main features
Scout	Scout	1.6 × 1.6 × 1.6		0:14	Automatic alignment
B_1 mapping	DREAM_B1	4.0 × 4.0 × 4.0	CAIPI 2 × 2_{z1}	0:05	Single-shot 3DREAM
B_0 mapping	B0	2.4 × 2.4 × 2.4		0:32	TE of 1.29, 3.09 ms
rs-fMRI	RestingState	2.4 × 2.4 × 2.4	CAIPI 1 × 6_{z2}	10:21	TE/TR of 30/570 ms, 3D-EPI with water excitation and semi-elliptical sampling, 1,070 volumes, initial one-time inversion recovery, 1 FID navigator/volume
T_1-weighted	T1	0.8 × 0.8 × 0.8	CAIPI 1 × 2_{z1}	6:35	4×TE: 1.6–6.5 ms, elliptical sampling, r.m.s. across TEs, MPRs (sagittal, coronal, axial), 1 FID navigator/TR
T_2-weighted	T2_caipi	0.8 × 0.8 × 0.8	CAIPI 1 × 2_{z1}	4:47	Elliptical sampling, MPRs (sagittal, coronal, axial) 1 FID navigator/TR
FLAIR	FLAIR	1.0 × 1.0 × 1.0	2 × 1	4:37	Elliptical sampling, MPRs (sagittal, coronal, axial)
Diffusion-weighted (CS-DSI)	DiffusionDSI_r DiffusionDSI	1.5 × 1.5 × 1.5	1 × 3	12:04	112 *q*-space samples, b_{max} = 6,800 s/mm^2
T_2*/susceptibility-weighted	QSMEPI_AP QSMEPI_PA	0.8 × 0.8 × 0.8	CAIPI 3 × 2_{z1}	6:20	6× TE: 7.4–31.9 ms, 4 averages per TE (24 images), 45 s per 3 rephased TE images, 1 FID navigator/10 TRs
T_2-weighted hippocampal subfields	T2_Hippocampal Subfields	0.4 × 0.4 × 1.6		6:29	Slices perpendicular to the long axis of the hippocampus (AutoAlign)
Body scout	BodyScout	5.0 × 5.0 × 5.0		0:15	Moving-table acquisition
Body fat	FatImaging	2.0 × 2.0 × 5.0		0:12	Breath-hold acquisition with automatic commands
				52:31	

All sequences provide whole brain coverage with isotropic resolution (except for the abdominal and hippocampal subfields imaging). PI accel: parallel imaging acceleration; TA: acquisition time. CAIPI: CAIPIRINHA undersampling pattern with a CAIPI shift along the second phase encoding direction. Data adapted from ref. 67.

been implemented. To maximize data consistency, none of the brain scans requires manual interaction for field-of-view (FOV) positioning. Instead, automatic alignment based on three-dimensional (3D) scout images and carefully predefined FOVs is used. Only the final abdominal fat/water MRI requires manual FOV positioning as described below. In the Rhineland Study, a marker-less motion tracking system[25–27] (TracInnovations) and sequence-specific, very fast MR-based free induction decay (FID) navigator[28] are further used to assess participant head motion. The latter may be used for future on-line motion tracking and prospective motion correction without an external tracking device. Furthermore, respiration and pulse traces are obtained throughout the entire protocol using an MR-compatible respiration belt and plethysmograph. These additional instruments to collect motion, respiration or pulse data can be employed while running the MRI scan protocol if the respective measurements are of interest for a specific research study.

MRI processing

Following MR image collection and transfer to the extensible neuroimaging archive toolkit[29] (XNAT) database management system, the acquired scans are input to dedicated processing pipelines designed for a single or a combination of different MR contrasts. The image processing pipelines of the Rhineland Study are based on the Nipype[30] framework, a Python-based open-source workflow engine, to integrate both in-house developed and existing state-of-the-art neuroimaging software tools. As the analysis pipelines comprise many interdependent steps that are performed by using various neuroimaging software tools and packages, the Nipype framework facilitates efficient interaction with different components or steps of the analysis pipelines. It also allows easy-to-use interfaces for seamless interaction with the neuroimaging software tools as well as flexibility to allow customization for specific requirements of some pipelines. Another advantage of the Nipype workflow is that the subsequent steps in a processing pipeline can be resumed from the point where it stopped if large number of participants are processed in a batch mode. The image processing pipelines exploit high-performance computing (HPC) and graphics processing unit (GPU) acceleration whenever possible to reduce the computational cost. HPC resources are extremely important

BOX 1

Additional details about the custom sequence variants used for the standard MR contrasts of the core MRI protocol

- The custom T_1-weighted multi-echo MPRAGE sequence combines CAIPIRINHA sampling (reducing parallel imaging noise penalty) and elliptical sampling (reducing the number of *k*-space echo readouts), which makes 0.8 mm isotropic resolution in 6:35 min acquisition time feasible[1]. The T_2-weighted SPACE sequence uses a similar strategy
- The specific multi-echo MPRAGE sequence variant[16] was chosen to allow for a T_1-weighted image with reduced geometric distortions matched to the T_2-weighted image[73] using a high-SNR r.m.s. echo combination
- The custom CAIPIRINHA 3D-EPI rs-fMRI sequence allowed us to achieve a high temporal resolution without overly strong parallel imaging as compared with a conventional simultaneous multislice EPI[18] as time-efficient fat-suppression and semi-elliptical sampling can be used[12]
- Performing simultaneous multislice diffusion-weighted MRI with a spin-echo echoplanar imaging sequence applying threefold slice acceleration[18,64,65] in combination with a CS-DSI protocol allows for an accelerated collection of 112 DSI scans with a maximum *b*-value of 6,800 s/mm^2 at 1.5 mm isotropic spatial resolution in 12 min acquisition time[14]. CS-DSI provides high radial resolution while maintaining high angular resolution and it is well-suited for analysis strategies that require high *b*-value acquisitions, therefore being a forward-looking dMRI acquisition strategy with a great potential for future developments
- The custom multi-echo T_2*-weighted sequence combines moderately high (sixfold) CAIPIRINHA parallel imaging with an EPI factor of 7, which results in three echo time whole-brain images at 0.8 mm isotropic resolution in only 45 s. However, this is repeated once with off-set TEs to result in six regularly spaced echo times between 7.4 and 31.9 ms. Corresponding data are acquired and averaged four times, resulting in 6:22 min acquisition time. This unconventional approach allows for valuable image-based corrections before averaging (e.g., retrospective motion and phase drift correction) and thus results in high-quality magnitude and phase images at 0.8 mm isotropic, even in participants with difficulties in lying still[15].

for efficient computing, which mainly depends on the underlying size and the amount of data acquired in a research project. In the field of epidemiology and neuroimaging studies, where large datasets from cohorts of participants are processed and analyzed, access to and harnessing HPC resources is of paramount importance. Therefore, with access to either institute-based computer clusters or external HPC facilities, researchers can substantially reduce the time required for data processing and effectively optimize complex computations involved in neuroimaging data analyses. In the Rhineland Study, we benefit largely from in-house compute nodes, each equipped with 48 dual cores and 4 GPU cards, making a total of 384 central processing unit (CPU) cores and 16 GPU units. These resources effectively serve to fulfil the demands of processing our weekly batches of imaging data, typically comprising up to 100 participants, with all the image analysis pipelines. Furthermore, for processing the entire cohort of participants simultaneously, we use the capabilities of our institute's HPC cluster comprising ~100 computer nodes each equipped with 72 CPU cores on average. A high number of cores will be beneficial in substantially speeding up the processing and facilitating the processing of large datasets in parallel. Likewise, the additional (yet for most pipelines optional) availability of GPUs will further enhance the processing speed of some pipelines, which benefit considerably from massive parallelization. Among all our processing pipelines, the dMRI and rs-fMRI processing pipelines are the most compute and memory intensive where multiple CPU cores, GPUs, and more than 64 GB of memory per node are required. We report processing times and memory requirements of all processing pipelines of the proposed MRI protocol in Table 2. As the analysis pipelines comprised different steps and different neuroimaging tools and thus require a great number of configurations in most cases, to ensure reproducibility and easy portability, we use Docker containers to encapsulate these pipelines together with the required tools and configurations. Dockerizing the pipelines avoids extensive re-configurations and compatibility issues and makes the complete pipeline portable to different other computing environments. As an alternative container framework to Docker, we also use Singularity, which has the ability to directly convert Docker images to Singularity images. Singularity is considered safer to run Docker images for scientific applications in an HPC environment that enables us

Table 2 | Overview of the input and output data to the processing pipelines of the MRI analysis protocol as well as the respective IDPs

Analysis pipeline	MRI input	Pipeline output	Imaging-derived phenotypes	Memory requirements	Processing time
FreeSurfer	T_1-weighted	Segmented volumes Standard FreeSurfer output at 1 mm isotropic Custom quality control images	Estimated cortical and subcortical volumes Thickness prediction of cortical structures	8–10 GB	CPU: 7–10 h
FastSurfer	T_1-weighted	Segmented volumes Standard FreeSurfer output at native input image resolution (0.8 mm isotropic) Custom quality control images	Estimated cortical and subcortical volumes Thickness prediction of cortical structures	6.5 GB	CPU: 3 h GPU: 1.3 h
WMH	T_2-weighted, T_1-weighted, and FLAIR images, and the standard output from the FreeSurfer processing pipeline	Segmented volumes Quality control images Statistics on segmented volumes	WMH load in vascular territories (e.g., posterior cerebral artery, middle cerebral artery, anterior cerebral artery, pons as part of the brainstem and cerebellum)	2–4 GB	CPU: ~90 min GPU: ~30 min
Olfactory bulb	T_2-weighted	Segmented volumes Quality control images Statistics on segmented volumes	Estimated volumes of the right and left olfactory bulb	6–8 GB	CPU: ~25 min GPU: ~2 min
Hypothalamus subfields	T_2-weighted and T_1-weighted pair, or standalone T_1-weighted	Segmented volumes Quality control images Statistics on segmented volumes	Estimated volumes of 24 structures, including 11 substructures of the hypothalamus and 13 adjacent structures	4 GB	CPU: 3 h GPU: <1 h
Hippocampal subfields	T_1-weighted and T_2 hippocampal subfields, or standalone T_2 hippocampal subfields	Segmented volumes Quality control images Statistics on segmented volumes	Estimated volumes of 28 structures, including 19 substructures of the hippocampus and 9 substructures of the amygdala	6 GB	CPU: 1.1 h
dMRI	DiffusionDSI, DiffusionDSI_r	Motion and distortion corrected dMRI data Quality control parameters from the motion correction CS-reconstructed DSI data Diffusion and microstructural parameter maps obtained from multiple dMRI models	Metrics describing the diffusion process and the underlying tissue microstructure, e.g., fractional anisotropy, mean, axial, and radial diffusivity obtained from the diffusion tensor model[68] Mean, axial, and radial kurtosis obtained from the kurtosis model[69] Neurite density index, orientation dispersion index, isotropic, intra- and extracellular volume fraction obtained from the neurite orientation and density imaging (NODDI) model[70]	18 GB	CPU: 1–1.5 h for distortion correction, 40 min/9 h/18 h for CS recon on 32/2/1 parallel threads) GPU: 3–5 h for motion correction, 30–90 min per MDT model fitting
rs-fMRI	RestingState, B0 Magnitude, B0 Phase, T_1-weighted	Cleaned fMRI image Custom quality control images Estimated rigid motion parameters	Functional connectivity matrix[71] System segregation index[72]	>64 GB	CPU: ~3–3.5 h
T_2*/susceptibility-weighted MRI	QSMEPI_AP, QSMEPI_PA, 12 magnitude and 12 phase images each	Six averaged magnitude and phase images for different TEs following preprocessing 1 SWI 1 R_2* map (1/s) + 1 amplitude map (a.u.) (from monoexponential R_2* fit on denoised magnitude data) Susceptibility map (ppm)	SWI: e.g., multiple sclerosis or cerebral small vessel disease lesions R_2* and susceptibility: e.g., deep gray matter iron content and white matter myelination	20 GB	CPU: 4.6 h (1 thread), 1.1 h (4 parallel threads)
Body fat imaging	Fat and water Dixon MRI	Segmented volumes Quality control images Statistics on segmented volumes	Estimated abdominal adipose tissue volumes composed of visceral and subcutaneous adipose tissue	6–8 GB	CPU: ~6 min

Estimates of the memory capacities required and the computation time using GPU and/or only CPU processing are listed per pipeline.

to harness the computational resources and accelerate large data processing. This combined Docker–Singularity approach offers us not only reproducibility but also easy portability to execute the analysis pipelines across other computing environments.

Functional MRI (fMRI), dMRI and multi-echo T_2*/susceptibility-weighted MRI require dedicated MR image-based preprocessing. The fMRI preprocessing pipeline corresponds to the standard statistical parametric mapping[31] (SPM) process and includes a specifically trained independent component analysis-based X-noisefier (FIX 1.06) classifier[32] provided by the Oxford Centre for Functional Magnetic Resonance Imaging of the Brain (FMRIB) to harmonize the current Rhineland Study resting-state fMRI (rs-fMRI) data with data from an initial sequence version that was more prone to a particular parallel imaging artifact. The dMRI pipeline includes retrospective motion and geometric distortion correction[33,34] adapted for diffusion spectrum imaging (DSI)[35] and subsequent compressed-sensing DSI reconstruction (CS-DSI)[36] of nonacquired diffusion spectrum samples[14,37]. The multi-echo T_2*/susceptibility-weighted pipeline applies retrospective motion and geometric distortion correction and additionally corrects for phase changes across eight individual measurements (45 s each). The preprocessing according to Stirnberg et al.[15] accounts for the fact that each measurement consists of three rephased echo time (TE) images and that the TEs of even-numbered measurements are interleaved with the TEs of odd-numbered measurements, resulting in six different TEs with four averages per TE (24 images in total). Final complex-valued averaging automatically compensates for partial-Fourier-related blurring and results in six echo time magnitude and phase images. In the Rhineland Study, subsequent computation of a susceptibility-weighted image (SWI), a quantitative susceptibility map (QSM) and a map of the effective transverse relaxation rate (R_2*) is performed using a third-party processing pipeline[38–41].

The complete MRI processing protocol includes multiple postprocessing pipelines to obtain MR image-derived phenotypes (IDPs). Among others, the IDPs include (Fig. 1) brain tissue volume, thickness and surface measures obtained across the whole brain or within regions of interest (e.g., cortical and subcortical structures, hippocampal subfields, hypothalamus, the olfactory bulb or brain lesions such as white matter hyperintensities (WMH) based on multimodal structural MRI[4–6,10,42,43], global and regional measures of the diffusive molecular transport and the underlying brain tissue microstructure based on diffusion-weighted MRI[14,44], brain functional connectivity using rs-fMRI[12] and volumes of subcutaneous and visceral adipose tissue based on a single-breath hold abdominal MRI[3]. On the basis of the T_1-weighted MR images, all brain structure volume, thickness and surface measures are obtained using the standard FreeSurfer processing pipeline[43,45] as well as the FastSurfer[5,6] processing pipeline, which is a novel and fast alternative to FreeSurfer that allows high-resolution MR image processing including additional subfields segmentation of brain regions such as the hypothalamus[42] and the cerebellum[46]. Innovative machine learning applications, particularly using deep learning, have been implemented within the structural MRI and body fat imaging processing pipelines of the protocol[3–6,10,42,46]. Our in-house tools have been designed and developed for the robust deployment in the large-scale population-based Rhineland Study, based on the study's research interests and the unavailability of reliable open-source tools for the automated segmentation and assessment of different brain tissue types such as abdominal adipose tissue, olfactory bulbs and hypothalamic substructures. They have, in part, already been successfully applied to other imaging datasets as well[47–49]. FreeSurfer was selected for whole brain and region of interest segmentation because it is a stable, reliable and well-supported neuroimaging framework that allows us to assess cortical as well as subcortical structures. Furthermore, FreeSurfer is used by other larger imaging populations cohorts (e.g., the Human Connectome Project[50], UK Biobank[51], Alzheimer's Disease Neuroimaging Initiative[52]), allowing us to replicate findings from these cohorts. However, it is important to note that also alternative image analysis pipelines can be run on the MRI data collected with the proposed protocol. For example, the SPM imaging framework was chosen in addition to FreeSurfer to process a subset of the Rhineland Study structural MRI data for solving one of the research questions of the respective study[53]. Moreover, we chose SPM for fMRI preprocessing as it offers a high degree of flexibility in terms of customization and parameter tuning and provides extensive documentation and support for troubleshooting due to its popularity in the neuroimaging community. Nevertheless,

in our investigations using fMRIPrep[54] as an alternative tool for fMRI preprocessing, we were unable to find any notable difference between the tools regarding image quality, robustness and downstream analysis, confirming the suitability of our MRI acquisitions for different processing strategies. The latter also holds for the dMRI acquisitions for which a wide spectrum of state-of-the-art diffusion processing and analysis techniques can be applied[14]. Among others, we selected the microstructure diffusion toolbox[44] for dMRI processing in the Rhineland Study because it incorporates a large set of models for dMRI microstructure analysis in one tool with the option for identical optimization routines to provide comparable model fitting. Furthermore, it enables GPU accelerated dMRI processing, which is indispensable in such a large-scale study.

MRI QA

To ensure high quality of the MRI acquisitions and extracted phenotypes, three stages of QA are implemented in the Rhineland Study within the proposed MRI protocol, as shown in Fig. 1. As a first stage, to ensure quality consistency and to detect potential malfunctions early on, a dedicated QA protocol is scanned every day on standardized phantoms. Box 2 provides additional details about this procedure. Secondly, a screening for incidental findings

BOX 2

Additional details about the phantom QA workflow

The QA phantom consists of a homogeneous gel mimicking brain gray matter. As phantom housing a cylindrical glass bottle was chosen to achieve a homogeneous main magnetic field (panel **a** of the image below, left side). To reproduce the phantom position inside the scanner over sites and sessions, a custom phantom mount (**a**, right side) was built (3D printed) that exactly fit the 64-channel head-neck coil (**a**, inset).

Phantom ingredients:

- 75.35% distilled H_2O
- 23.0% polyvinylpyrrolidon K30
- 1.0% agarose NEEO
- 0.65% NaCl Phantom specific

MR parameters:

- T_1 = 1,328 ms
- T_2 = 70 ms
- C = 0.61 S/m
- Apparent diffusion coefficient = $1{,}000 \times 10^{-6}$ mm^2/s

The phantom QA scans are acquired each day after the last participant, to be able to detect data inconsistencies and hardware defects as soon as possible. This ensures high-throughput data collection with minimal data loss. The QA protocol matches exactly the in vivo MRI scan protocol of the Rhineland Study. In addition to the proposed MRI scan protocol, a GRE scan (two measurements for SNR analysis[74]) is acquired with head and body coil. The GRE imaging data are saved uncombined (per receive channel) to get detailed information about the individual receive channels.

The acquired data are sent to an XNAT server by the technicians. The QA processing on the imaging data is performed using an in-house developed, fully automated processing pipeline implemented in Nipype[30]. The incoming data are converted to the NIfTI image format and the image header information is checked for protocol consistency (i.e., TE, TR, FOV, etc.) and system consistency (i.e., resonance frequency, RX/TX/gradient adjustments). The pipeline further incorporates an fBIRN[75] pipeline to analyze the EPI data and the diffusion tensor fitting program of the FSL[76] toolbox to process the diffusion-weighted MRI scans. The additional GRE scans are used to generate receive sensitivity maps, channel contribution maps and SNR maps. For each phantom-specific MR parameter map of the QA pipeline, mean and s.d. are computed across voxels within a region of interest (white) in the center of the phantom bottle (gray) as depicted in **b** for the collected localizer image and longitudinally assessed over time and sites. Reference mean and s.d. values are determined based on the distribution of all previous measurements of a QA metric. New measurements within the range of two s.d. around the mean, between two and three s.d. around the mean or outside these confidence intervals are marked as PASSED, WARNING or with a red flag, respectively (**c**). The results are stored in a JSON file and saved together with a final report and the summary images in the corresponding scan session on the XNAT system. After completion of this fully automated QA pipeline, the phantom scans are visually inspected by an MR physicist or technician in cases in which a warning or red flag was assigned to determine, after data integrity is ensured, whether a problem with the MR system exists. If so, further support from the vendor should be requested. As an example, in September 2023 a single channel (41) of the receive head coil broke (**c**, bottom row). This was noticed early on because the mean MPRAGE signal time course is monitored over the region of interest (**c**, top row). After replacement of the complete head coil all parameters were within the specified limits again. Note that the broken receive channel would not have been picked up by QA metrics examining all receive channels simultaneously.

(continued from previous page)

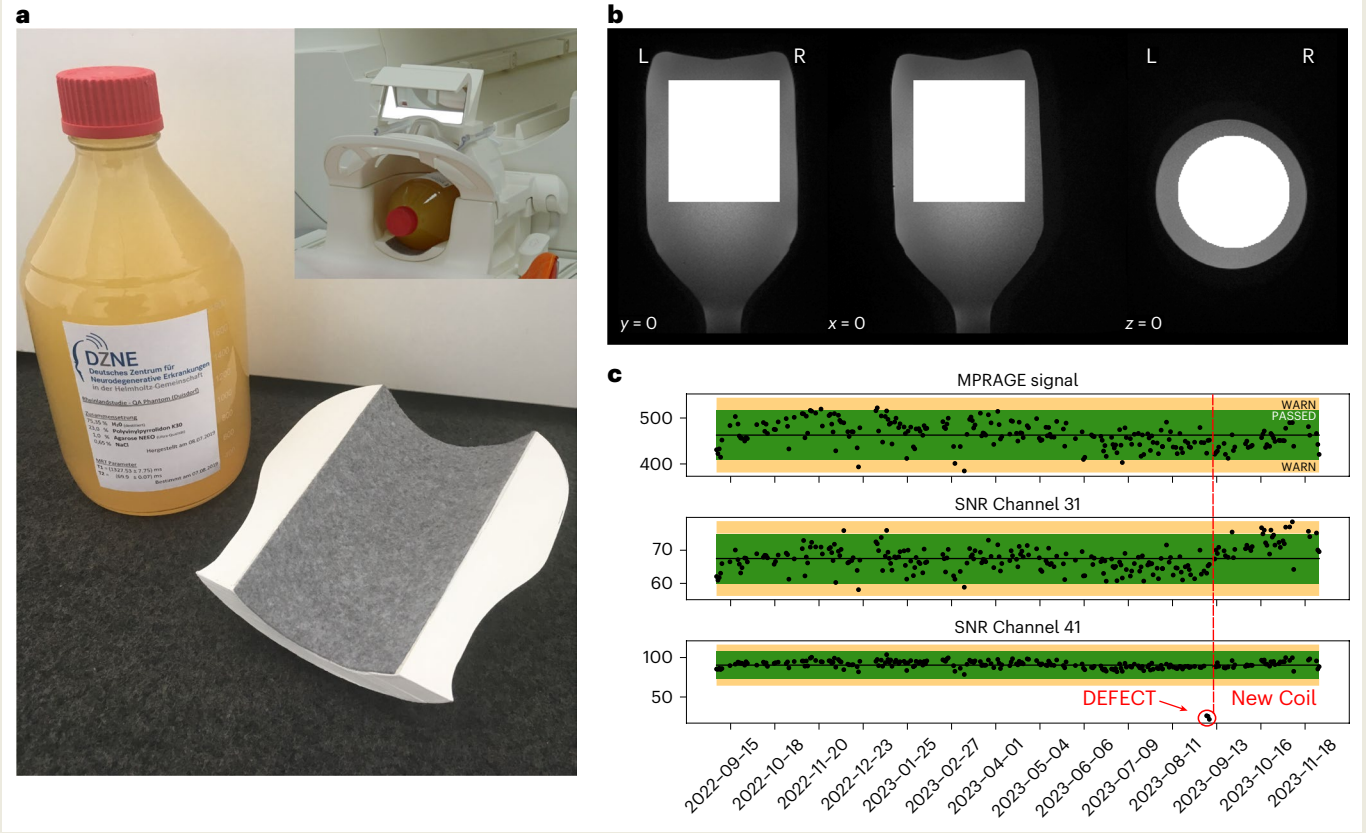

and a visual image quality rating is performed on all structural MRI scans before any image processing[9]. In addition, the completeness of the MRI acquisition protocol is evaluated though inspection of the MRI metadata and comments placed by the operator performing the MRI examination are checked. In this step, repeated measurements of the same MR contrast, e.g., due to imaging artifacts or technical issues, are also removed from the scan session. Thirdly, we run dedicated QA workflows that are specific to each MRI modality and postprocessing pipeline but use similar strategies and metrics for QA and rating of the MRI data and IDPs. During this QA stage, problematic data are identified automatically based on three different outlier selection criteria: visual quality warning or incidental finding as determined during the second QA stage, age-based outliers derived from the distribution of participant-specific QA metrics with respect to the population average[55] and a selection of random cases. All outliers are visually inspected by trained raters to decide upon their inclusion or exclusion from the dataset, which is subsequently made available for further research analysis. All metrics used to automatically identify outliers for QA are output measures of the processing pipelines as reported in Table 2, including, for example, FreeSurfer derived volumetric measures (Box 3, Fig. 2), dMRI model parameters such as fractional anisotropy and mean diffusivity, and pipeline-specific motion estimates such as the root-mean-squared (r.m.s.) movement of all intracerebral voxels with respect to a reference image[34]. As an example of such a pipeline-specific QA workflow, Box 3 and Fig 2. presents a detailed overview of the QA grading for the FreeSurfer processing pipeline. The overall MRI QA workflow described here was designed and developed within the framework of the Rhineland Study and can serve as a recommendation, but alternative QA tools and workflows that meet the specific requirements of the respective research study of interest can also be applied to the data collected and processed with the proposed MRI protocol.

BOX 3

Additional details about the QA workflow for the FreeSurfer processing pipeline

T_1-weighted MR images acquired with the MRI scan protocol are subsequently processed using the standard FreeSurfer processing pipeline (http://surfer.nmr.mgh.harvard.edu/) to obtain whole-brain segmentations. As part of the pipeline QA workflow, a subset of FreeSurfer outputs are visually inspected and a segmentation quality grading is given. This subset is selected based on incidental findings, examination warnings and a percentage of random cases. In addition, we use the within-cohort volumetric age dependency to identify participants outside of two s.d. of the expected population volume.

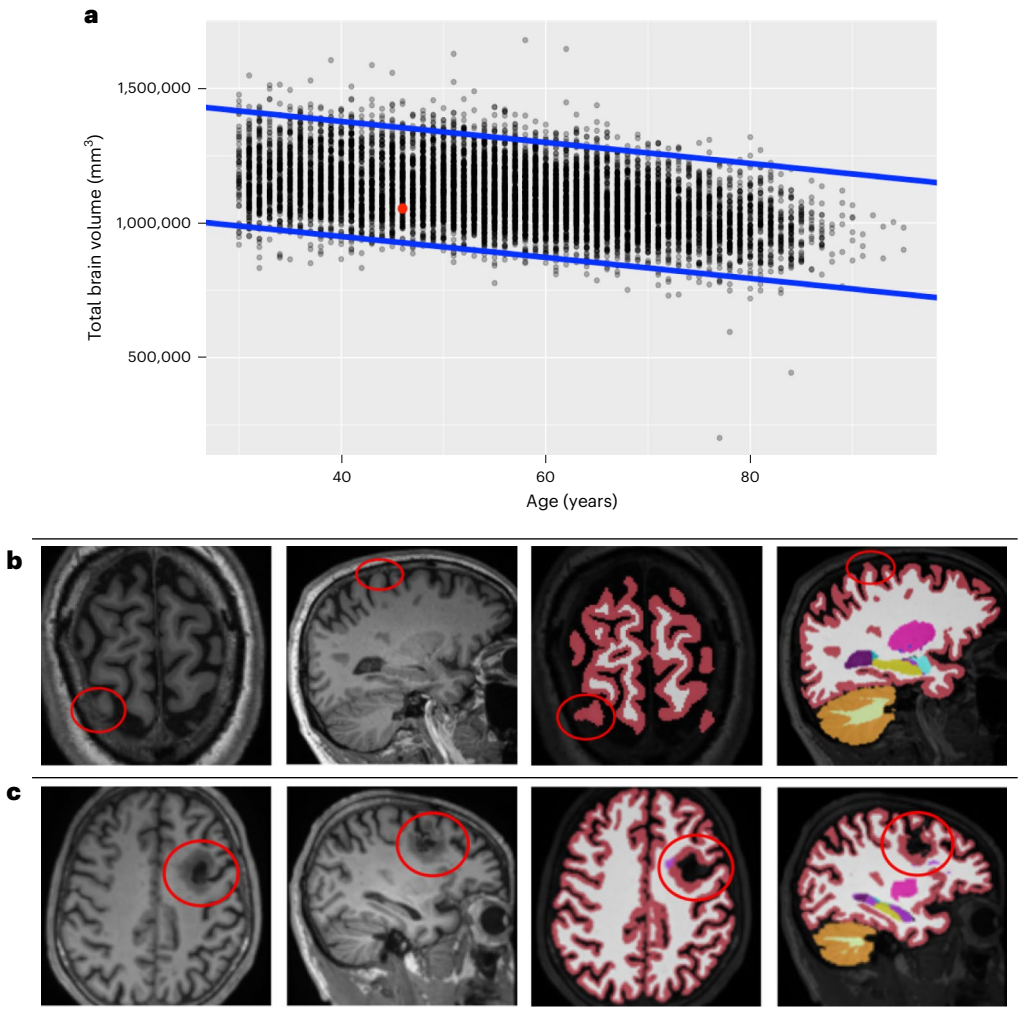

This approach is based on a simple linear model with respect to age. The FreeSurfer volume estimations used in this step are total brain volume, total cerebral white matter volume, total gray matter volume, ventricle volume, total intracranial volume and the ratio of the volumes for the left and right hemisphere. In the graph above, **a** presents the cohort volumetric age dependencies for total brain volume. An outlier was identified and further visually inspected when any of the preselected FreeSurfer output estimates fell outside two times the linear model's s.d. (depicted by blue lines). The red dot on the graph represents the participant under investigation.

QA grading is performed by visually inspecting the raw T_1-weighted MR images and its FreeSurfer segmentations on snapshots of two anatomical views. The QA grading is given based on the segmentation accuracy of seven brain structures groups: cerebral cortex, cerebral

(continued from previous page)

white matter, basal ganglia, ventricles, hippocampus and amygdala, thalamus and cerebellum. For each group, the QA flag can be either PASS or FAIL. A PASS flag is given when there is a correct segmentation output or minor errors (**b**) and FAIL when severe segmentation errors occur (**c**). Specifically, **b** shows a PASS example of slight oversegmentation of the right posterior frontal cortex. The cortex segmentation includes the dura mater (as shown by the red circle). However, the segmentation error is present in fewer than five consecutive slices. Consequently, it is considered a minor error, and the cortex segmentation is flagged as a pass. Whereas **c** presents a FAIL example of oversegmentation of the cerebral cortex in the area of a brain lesion (red circle). Afterward, an overall QA is assigned as PASS, FAIL or PARTIAL based on the individual grading of the seven above mentioned QA flags if they are labeled all as PASS, FAIL or a combination of both, respectively.

Expertise needed to implement the protocol

The proposed MRI acquisition and processing protocol was designed and developed by a multidisciplinary team of experts with knowledge in the fields of MR physics, computer science and epidemiology. For its successful implementation and execution in other research studies, however, less expertise is needed. The most training and experience is required for the first major part of the modular protocol, the MRI acquisitions. An experienced MRI operator must perform the in vivo MRI examinations; however, no additional expertise is required compared with the technical staff of any study running MRI examinations, regardless of the application of this specific MRI scan protocol. Only a few manual adjustments are required from the MRI operator during the examination, specifically only for the abdominal MRI, which are described in detail in the corresponding step of the scanning procedure. The technical infrastructure to manage and store large-scale MRI data and related metadata should be set up by IT personnel. For setting up and running a basic XNAT platform, support of IT staff would only be required if the neuroimaging researchers lack sufficient background knowledge and experience in Linux operating systems. However, the maintenance and extension of the XNAT resource, depending on the research goals and the size of the research data, requires a dedicated IT specialist to provide continuous support on storage requirements, data backup, security and data sharing. The execution of the processing pipelines, the second major part of the MRI protocol, only requires basic knowledge in computer science and the ability to use the command line. By design, this part of the protocol avoids extensive reconfigurations or manual installation of required software, thereby facilitating its implementation and reducing the expertise needed.

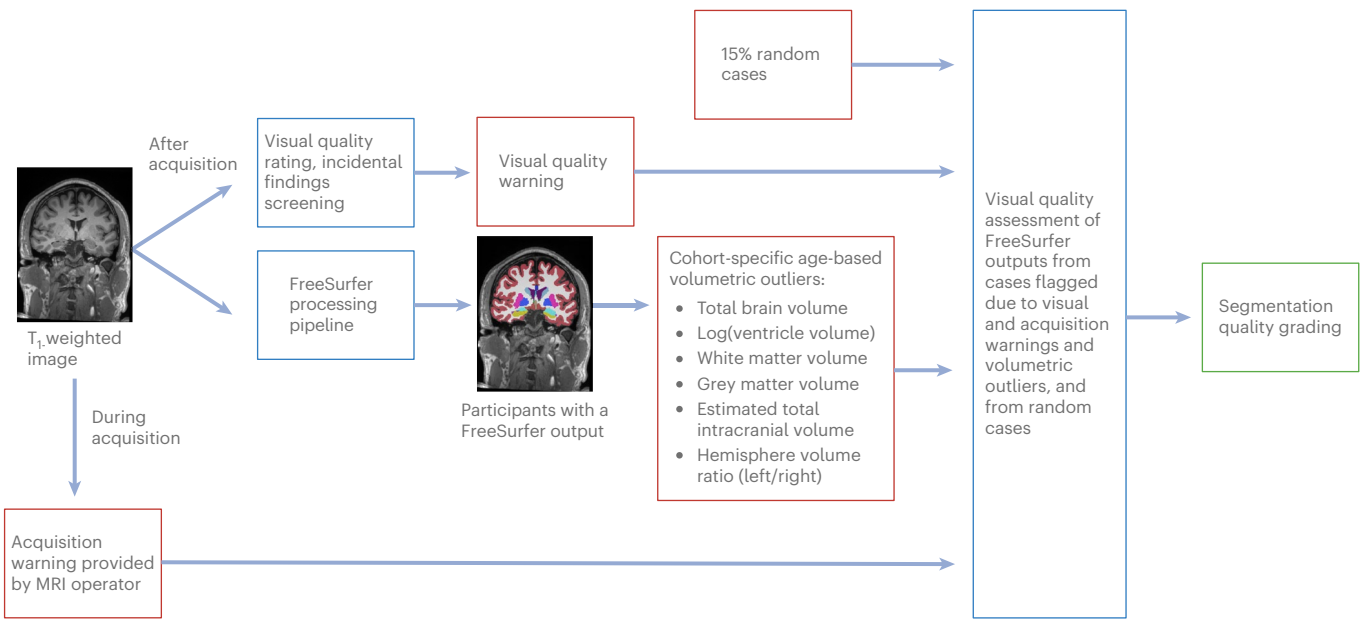

Fig. 2 | QA workflow for the FreeSurfer processing pipeline. As part of the pipeline QA workflow, a subset of FreeSurfer outputs are visually inspected and a segmentation quality grading is given.

Depending on the size of the imaging study and the amount of MRI data collected, however, expertise in HPC might be useful to speed up the data management and processing. No specific background in MRI processing or machine learning is needed. Documentation and an example dataset are provided to get familiar with the input and output of the different processing pipelines. For the QA of the acquired MRI data and IDPs, expert evaluation is required. If desired, a radiologist or trained neuroscientist with sufficient knowledge about brain anatomy should screen the structural scans for incidental findings[9]. Raters with pipeline-specific knowledge (e.g., about brain anatomy, the effect of motion and other acquisition-related artifacts on MRI scans) must be trained for visual QA and the inherent manual quality rating. The different aspects of a recommended QA workflow have been described in detail within this protocol.

Applications of the protocol

This modular MRI protocol was designed and developed for large-scale prospective population imaging and optimized to provide versatile high-resolution and high-quality imaging data in a short scan time. The scan protocol forms the first major component of the overall MRI protocol and its specific MRI sequences were custom developed to improve the data quality beyond what is commonly available so far. The image analysis protocol includes innovative processing pipelines based on machine learning, particularly deep learning, for the assessment and quantification of specific imaging phenotypes. To complete the overall MRI protocol, integrated QA pipelines are implemented to ensure high quality of the imaging data and extracted phenotypes. It is worth highlighting that all the MRI acquisition and analysis methods of the MRI protocol are adaptable and generally applicable and not geared toward a specific disease. Thus, the proposed protocol may be of specific interest for a wide range of neuroimaging applications.

The overall MRI protocol has already been successfully applied for the past few years for population neuroimaging in the Rhineland Study (ongoing, currently more than 11,000 participants, target participant number of 20,000), its target application. We therefore recommend it for upcoming long-term and large-scale prospective population imaging studies of both cross-sectional and longitudinal research design. Its application by other cohorts will enhance comparability and exchange between research studies.

Neuroscientists setting up research or clinical studies are at liberty to trim the protocol to their needs by only implementing single components of the modular MRI protocol. In fact, subsets of the protocol's MR contrasts and respective analysis methods have been and are being used in several clinical research settings because of the improved performance over more common imaging protocols. These studies investigate, e.g., cerebral small vessel disease, SARS-CoV-2 infection[47], attention-deficit/hyperactivity disorder[56], brain volume changes after infarcts[57,58] or cognitive impairment in chronic heart insufficiency in patients. The scan protocol has also already been implemented for neuroimaging in the general population, more specifically for fMRI and multiparametric mapping in a recent long-term study[59] and for fMRI in a longitudinal intervention study[60,61]. Moreover, the proposed MRI scan and analysis protocol has been adapted for another scanner of the same vendor, the MAGNETOM Skyra, to be used in clinical multisite studies, such as the currently recruiting HIFI-CAA cohort study investigating brain alterations in cerebral amyloid angiopathy (CAA) through high-frequency MRI (HIFI). Ongoing research or clinical studies that already collect MRI data with a highly comparable imaging protocol can benefit from this modular MRI acquisition protocol, specifically the image analysis protocol and its fully automated processing pipelines[47–49] as well as the multistage QA procedures to facilitate QA and study harmonization.

Advantages, limitations and alternative methods

Using the proposed MRI protocol, a more versatile set of MR contrasts with higher resolution than is usual to date is directly linked to fast and fully automated, adaptable and expandable QA and data analysis pipelines.

This protocol provides a forward-looking, but also mature, MRI acquisition strategy for a wide range of research studies. It uses findings of recent popular imaging studies such as the original Human Connectome Project[50] on the advanced technology of high-performance MRI

scanners to achieve impeccable image quality, while additionally focusing on time-efficient accelerated MRI. Furthermore, the proposed scan protocol covers a more versatile set of neuroimaging MR contrasts at higher image resolution than the one of the well-established UK Biobank[51] study, while still being comparable and thus facilitating research across large-scale population imaging studies.

Incorporating the concept of the free protocol, the proposed MRI protocol uniquely enables innovations at the level of acquisition and methods development within the framework of an ongoing large-scale population study.

The modular structure of the MRI protocol makes it suitable for a wide range of neuroimaging applications. On request, MRI sequences can be readily shared with other research collaboration partners. Likewise, all postprocessing pipelines are designed for easy distribution. If the protocol's hardware and software requirements are met, this allows for high research reproducibility, thus enhancing comparability and exchange between research studies and facilitating study harmonization.

The MRI sequences in this protocol are designed and optimized for the MAGNETOM Prisma MRI scanner (Siemens Healthineers) running software version VE11C. At the time of study launch, the scanner had a stronger than average gradient system of 80 mT/m at 200 T/m/s slew rate. The corresponding image analysis pipelines expect, as input, images acquired with those sequences and hardware (e.g., 64 channel head–neck coil). When changes in hardware or software are inevitable, they must be considered cautiously for consistent outcomes. For instance, CAIPIRINHA parallel imaging undersampling factors of up to six require a suitable receive coil such as the 32 channel head coil, but not the 24 channel head–neck coil distributed by the same vendor.

An adapted MRI protocol for harmonized data collection across sites with less performant scanners of the same vendor has already been developed on a MAGNETOM Skyra (45 mT/m at 200 T/m/s, 32 channel head coil) using identical custom sequences. For most of them, all parameters could be copied and parallel imaging did not have to be changed for any of them. Minor adaptions were only required for rs-fMRI to maintain TE and volume repetition time (TR) and T_2*/susceptibility-weighted imaging to keep TE and TR comparable (TE of 6.9–32.4 ms, TR of 53.3 ms, echo-planar imaging (EPI) factor 5, TA of 9.2 min). A major change of image resolution was only required for dMRI to maintain TE and TR and, largely, the diffusion encoding scheme up to the largest *b*-values (2.0 mm instead of 1.5 mm isotropic resolution, 72 instead of 93 slices). Therefore, all processing pipelines of the proposed MRI protocol are compatible to analyze MRI data collected at the Skyra, except for the dMRI pipeline. A combined analysis of Prisma and Skyra dMRI data would be possible, but requires a modified analysis pipeline and downsampling (1.5 mm to 2.0 mm) of the Prisma data. Note that although the amount of signal decay due to intravoxel dephasing depends on the original image resolution, it is not altered by the downsampling procedure, highlighting a limitation in comparing downsampled data with originally low-resolution data. However, the effect of intravoxel dephasing could be matched by storing the complex raw MRI acquisitions and downsampling the data via the fast Fourier transform and a pruning of the outer *k*-space.

Compatibility with more recent software for the same scanners (VE11E) has already been verified. Support for the most recent scanner generation of the same vendor (NumarisX) is currently under investigation as a necessity for a wider application besides the Rhineland Study. For instance, in an upcoming national multisite study, the Rhineland Study sequences and (compatibility) protocols are going to be used with data harmonization and high scan efficiency in mind. At the time of writing, among 15 of the participating scanners, 3 use Numaris X and 12 use VE11 baselines; however, the number of scanners running Numaris X is expected to increase. A subset of sequences has already been ported successfully. As soon as all sequences are ported and thorough testing is complete, they are going to be released publicly along with the VE11 sequences as well. Alternatively, adapting the scan and analysis protocol for other scanners or reproducing the entire scan protocol using vendor-provided default MRI sequences that still lack some of the involved state-of-the-art technique is, at present, only possible to a limited degree.

The protocol and analysis pipelines were designed for use in large-scale population studies. Special care should be taken when applying the MRI analysis protocol to process imaging

data from participants presenting gross brain abnormalities or severe pathology, which may cause inaccuracies or failure of MRI processing pipelines due to poor image qualities. Thus, automated QA procedures and manual inspection of flagged problematic cases are of great importance.

Regulatory approvals

Before the use of the proposed MRI protocol in an imaging study involving human participants, approval must be obtained from the appropriate local ethical review board. All MRI scans must be acquired according to institutional and national regulations with written informed consent from the participants of the study.

The proposed MRI sequences are investigational and not for diagnostic or commercial use. To request the download of sequence binaries, the receiving institution has to register as a user of the Siemens (Healthineers) Core Competence Partnership (C2P) exchange platform. Agreeing to the terms and conditions of both Siemens and the sequence providers is required. The former settle the legal preconditions to install and run investigational pulse sequences. The latter additionally specify how the sequence providers shall be acknowledged by the receiving institution according to good scientific practice.

Materials

Human participants

The proposed MRI protocol has been successfully applied in over 11,000 participants of the Rhineland Study (www.rheinland-studie.de), an ongoing community-based prospective cohort study with a target participant number of 20,000 that invites inhabitants aged 30 years and above at baseline living in two geographically defined areas in the city of Bonn, Germany. Persons living in these areas are predominantly German with Caucasian ethnicity. The sole exclusion criterion is insufficient German language skills to provide informed consent.

▲ **CAUTION** Approval to undertake the study was obtained from the ethics committee of the Medical Faculty of the University of Bonn. The study is carried out in accordance with the recommendations of the International Council for Harmonization Good Clinical Practice standards(ICH-GCP). Written informed consent was obtained from all participants in accordance with the Declaration of Helsinki.

Equipment

- MRI scanner
- MRI receive coil
- MR-compatible screen
- MRI data storage system, e.g., XNAT
- Computing hardware

  ▲ **CRITICAL** We recommend using a powerful workstation for HPC to manage and process the acquired MRI data. An efficient personal computer might be suitable if only some modules of the processing protocol are required and no extensive parallel computing of multiple participants is of importance. As a minimum set of requirements for processing the protocol data with all the processing pipelines, a workstation with similar configurations to the following is recommended, which has Intel Xeon Gold 6130 @ 3.00 GHz 2 × 12 (hyperthreading enabled) processing cores, 96 GB of main memory and 2× Nvidia Quadro P5000 GPUs.

Equipment setup

MRI scanner, sequences and data storage

The Rhineland Study MRI acquisition protocol runs on two identical 3T Siemens MAGNETOM Prisma MRI scanners (Siemens Heathineers) equipped with a 80 mT/m at 200 T/m/s gradient system and a 64-channel head–neck coil. All custom sequences were implemented and all

parameters were optimized for the scanner software version VE11C. An overview of the most relevant MRI sequence parameters is given in Table 1. During the rs-fMRI sequence, a fixation cross is displayed on a 30 inch MR-compatible OptoStim screen (Medres) located in the scanner room. A file containing the image of the fixation cross is distributed together with our publicly available example dataset.

We use the XNAT platform for storing and organizing all the MRI data together with output data derived from the analysis pipelines. XNAT provides the required platform and offers flexibility by supporting nonimaging data types such as other auxiliary data from the scanner or the analysis pipelines. We benefit largely from the extensibility of XNAT through its plugins architecture and automate the minimum preprocessing such as the DICOM series to NIfTI file format conversions, the QA of acquisition parameters and the extraction of metadata for documentation purposes right after the scan sessions are archived. Its continuous development and support status since the launch of the Rhineland Study several years ago, and its robust set of features and extensive capabilities aligning with the needs of our long-term study set a solid foundation to adopt the XNAT platform for our neuroimaging data management requirements. Similar alternative platforms might have also evolved and improved over time and could be used if they meet the specific requirements of the research projects.

Software

To setup the MRI acquisition according to the proposed protocol, all MRI sequence protocol parameters are available on GitHub (https://github.com/mrphysics-bonn/mri-protocols/tree/main/rhineland-study) and all custom MRI sequence and image reconstruction binaries are provided for various IDEA (Siemens Healthineers) software baselines via Siemens' C2P exchange platform.

The processing pipelines of the protocol required to process the collected MRI data are provided on GitHub (https://github.com/orgs/RhinelandStudy/repositories) and should be executed as described in the procedure via containers using Docker or Singularity that encapsulate all necessary software required to run a particular pipeline.

Estimates of the memory capacities required for data processing are reported in Table 2.

The NIfTI image file format is the required input format of the image analysis pipelines of the proposed MRI protocol. The conversion of all DICOM acquisitions to the NIfTI file format can be automated using the XNAT plugins architecture, or dedicated software such as, for example, the dcmstack converter (https://github.com/moloney/dcmstack).

Example dataset

A single dataset was acquired for one healthy volunteer (male, 34 years old) using the proposed MRI scan protocol and is publicly available for download from the Zenodo data sharing platform[62]. Two zip files are provided storing the raw MRI acquisitions (Table 1 and Fig. 3) and the output data of a set of processing pipelines (Table 2) from the MRI protocol. This example dataset should support the user in becoming familiar with the input and output of the different processing pipelines shared with the proposed MRI protocol.

Procedure

MRI data acquisition

● **TIMING ~70 min in total per examination from the arrival to the departure of the participant, including ~10 min for participant transfer and positioning in the scanner and ~60 min of MRI scanning**

▲ **CAUTION** Participants with contraindications or exclusion criteria are not eligible to undergo the MRI examination[8].

▲ **CAUTION** Written informed consent to participate in the research study needs to be obtained from the participant before the MRI examination.

▲ **CRITICAL** Enough time for participant preparation and scanning needs to be reserved for the examination at the MRI scanner.

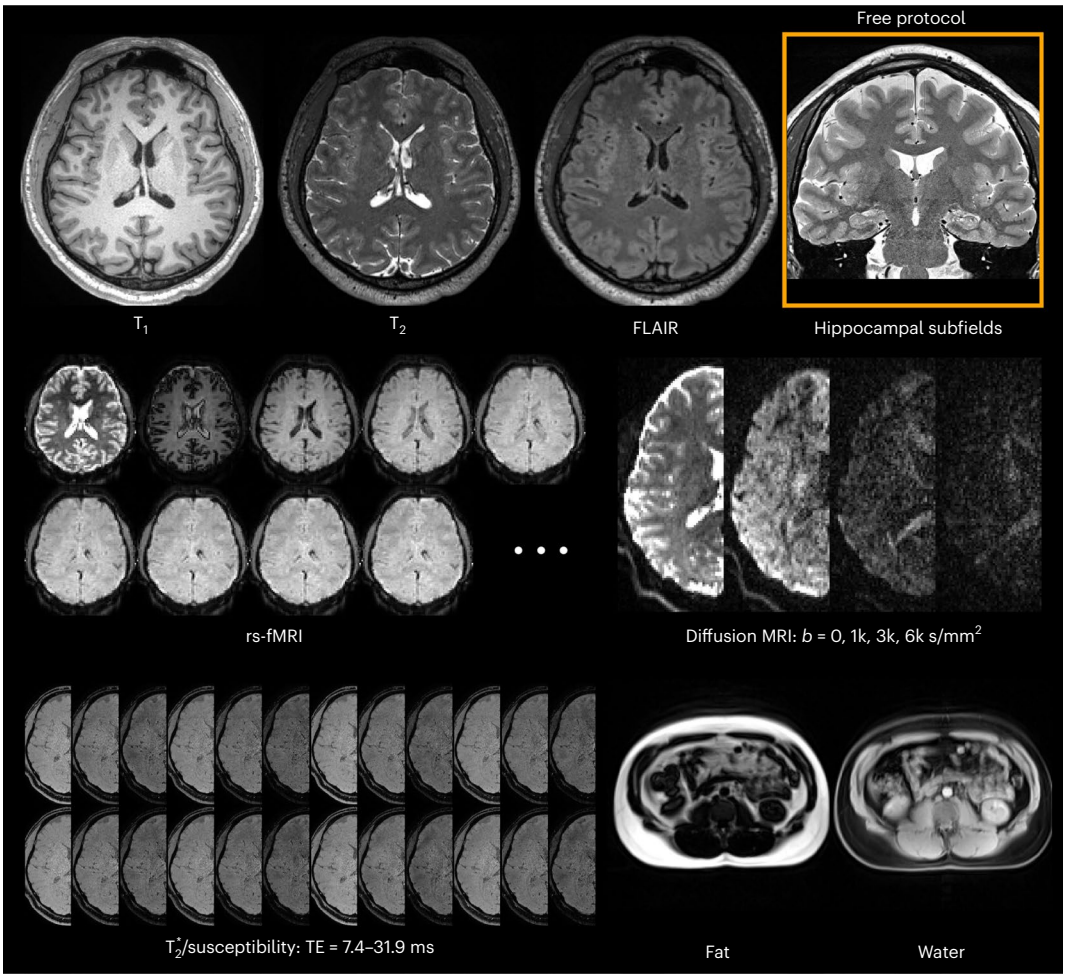

Fig. 3 | Overview of the output of the MRI acquisition protocol. Representative views of the unprocessed MRI data collected using the MRI acquisition protocol. Top: T_1- and T_2-weighted images, the FLAIR acquisition and the high-resolution hippocampal subfields imaging data. Middle: the rs-fMRI data (first 9 out of 1,070 images showing one-time inversion recovery) and a $b = 0$ scan without diffusion weighting and diffusion-weighted images for $b = 1{,}000$, 3,000 and 6,000 s/mm^2. Bottom: the raw T_2*/SWIs at six distinct TEs and body fat imaging data.

1. Position the participant in the MRI scanner. This is not different from any other MRI examination for neuroimaging and should be performed by a qualified MRI operator following the MRI center's guidelines to ensure the participant is situated comfortably in the head coil for the scan time of ~1 h.
   ▲ **CAUTION** A 3T MRI scanner has a strong magnetic field. Ferromagnetic material in the scanner room can cause injuries and is prohibited. Only MR-compatible equipment is allowed in the scanner room.
2. Perform head scout. A rapid T_1-weighted 3D spoiled gradient echo (GRE) sequence is applied at 1.6 mm isotropic resolution (TA of 14 s, TR of 3.15 ms, TE of 1.37 ms, flip angle 8°, FOV of 260 × 260 mm, 128 sagittal slices). From this 3D image, the reference space for automatic slice positioning of all subsequent head MRIs is calculated automatically.
   ◆ **TROUBLESHOOTING**
3. Acquire B_1 field map. A single-shot 3D dual refocusing echo acquisition mode (DREAM) sequence[2,63] is applied at 4 mm isotropic nominal resolution (TA of 5.4 s, TE of 1.12, 2.03 ms, preparation flip angle 59°, flip angle 6°, FOV of 216 × 216 mm, 48 sagittal slices). From the two magnitude images, a flip angle map and an ideal reference voltage map are calculated automatically.

4. Acquire B_0 field map. A 3D dual-echo spoiled GRE sequence is applied at 2.4 mm isotropic resolution (TA of 32 s, TR of 6 s, TE of 1.29, 3.09 ms, flip angle 6°, FOV of 216 × 216 mm, 60 oblique axial slices). From the two phase images, a B_0 map is calculated automatically.
5. Acquire rs-fMRI. A 3D EPI sequence with variable echo train lengths and water excitation is applied to collect rs-fMRI data at high temporal resolution (TA of 10.5 min, TR of 570 ms, TE of 30 ms, inversion time (TI) of 240 ms, flip angle 16°, FOV of 216 × 216 mm, 60 oblique axial slices).
   ▲ **CRITICAL STEP** During the rs-fMRI scan, the participant must look at a fixation cross.
   ◆ **TROUBLESHOOTING**
6. Acquire T_1-weighted MRI. T_1-weighted images are acquired at 0.8 mm isotropic spatial resolution using a multi-echo magnetization prepared rapid gradient-echo (ME-MPRAGE) sequence with elliptical sampling (TA of 6.5 min, TR of 2,560 ms, TE of 1.68, 3.29, 4.90, 6.51 ms, readout pixel bandwidth 740 Hz, TI of 1,100 ms, flip angle 7°, FOV of 256 × 256 mm, 224 sagittal slices). From the four echo time magnitude images, one r.m.s. magnitude image is calculated automatically. Bandwidth-matching to the T_2-weighted acquisition (next step) ensures that both images perfectly register, e.g., for joined T_1–T_2 segmentation or T_2-informed dura removal from T_1. From the r.m.s. image, multiplanar reconstructions (MPR) at 2.5 mm slice thickness along coronal, sagittal and axial slice direction are calculated automatically.
7. Acquire T_2-weighted MRI. T_2-weighted images are acquired at 0.8 mm isotropic spatial resolution using a 3D TSE sequence for sampling perfection with application-optimized contrasts by using flip angle evolution (SPACE) with elliptical sampling (TA of 4.6 min, TR of 2,800 ms, TE of 405 ms, readout pixel bandwidth 744 Hz, FOV of 256 × 256 mm, 224 sagittal slices). From the magnitude image, MPR at 2.5 mm slice thickness along coronal, sagittal and axial slice direction are calculated automatically.
8. Acquire FLAIR MRI. T_2-weighted FLAIR images are acquired at 1.0 mm isotropic spatial resolution using a 3D T_2 FLAIR sequence with elliptical sampling (TA of 4.5 min, TR of 5,000 ms, TE of 393 ms, TI of 1,800 ms, FOV of 256 × 256 mm, 176 sagittal slices). From the magnitude image, MPR at 2.5 mm slice thickness along coronal, sagittal and axial slice direction are calculated automatically.
9. Acquire diffusion-weighted MRI. Simultaneous multislice dMRI is performed with a spin-echo EPI sequence applying threefold slice-acceleration[18,64,65]. The CS-DSI protocol is used to collect dMRI scans at 1.5 mm isotropic spatial resolution (TA of 12.1 min, TR of 5,500 ms, TE of 105 ms, FOV of 210 × 210 mm, 96 slices, b_{max} = 6,800 s/mm^2, Δ = 49.5 ms, δ = 19.7 ms).
   ▲ **CRITICAL STEP** This acquisition consists of two scans: four non-diffusion-weighted images with reversed (posteroanterior) phase encoding are required for distortion correction during image postprocessing and must be acquired before the CS-DSI scan with anteroposterior phase encoding, TA includes both scans.
10. Acquire T_2*/susceptibility-weighted MRI. A highly segmented GRE 3D EPI sequence with six echo times is applied for motion-robust, rapid quantitative susceptibility and R_2*mapping. This sequence collects imaging data at 0.8 mm isotropic spatial resolution using skipped-CAIPI sampling (TA of 6.3 min, TR of 51.1 ms, TE of 7.4, 12.3, 17.2, 22.1, 27.0, 31.7 ms, flip angle 20°, EPI factor 7, FOV of 216 × 216 mm, 176 sagittal slices). This acquisition consists of two identical scans, except for the phase encoding direction: anteroposterior phase encoding is performed first, posteroanterior phase encoding is performed second, TA includes both scans.
11. Acquire high-resolution T_2-weighted hippocampal subfields MRI. T_2-weighted images are acquired at 0.4 × 0.4 × 1.6 mm resolution using a 2D TSE sequence. The large voxel dimension is oriented approximately along the long axis of the hippocampus (TA of 6.5 min, TR of 7,930 ms, TE of 44 ms, turbo factor 9, FOV of 224 × 189 mm, 45 oblique-coronal slices).
    ◆ **TROUBLESHOOTING**
12. Prepare for body scout. Inform the participant of the now-following movement of the MRI table. The participant is also prepared to listen to the breath-hold commands automatically played through the MRI intercom synchronized to the beginning and end of the abdominal MRI that will be performed after the body scout scan.
    ▲ **CRITICAL STEP** The participant must hold their hands close to their body. Crossing of the arms (on the stomach) is not allowed.

13. Perform body scout. A moving-table 2D GRE sequence is applied at 5 mm isotropic resolution (TA of 15 s, TR of 2.56 ms, TE of 1.44 ms, table velocity 46 mm/s, FOV of 480 × 420 mm, 138 axial slices).
14. Prepare for body fat imaging. On the basis of the body scout image, the center slice of the subsequent abdominal MRI is positioned manually on the middle of the third lumbar vertebra.
15. Acquire abdominal MRI. Abdominal MRI is performed for 72 axial slices using a breath-hold two-point Dixon 3D spoiled GRE sequence at 2 × 2 × 5 mm resolution (TA of 12 s, in-plane spatial resolution 2.0 mm^2, slice thickness 5 mm, TR of 4.12 ms, TE of 1.23, 2.46 ms, FOV of 500 × 437 mm, flip angle 6°, readout pixel bandwidth 750 Hz). The arms of the participant are placed at side. From the fat and water 'in-phase' and 'opposed-phase' images, a 'water' and a 'fat' image are automatically computed.
    ◆ **TROUBLESHOOTING**
16. Lead the participant out of the scanner room. After the MRI examination has finished, help the participant out of the scanner and the scanner room.
17. Save the acquired MRI data. Transfer all acquired imaging data from the scanner to the XNAT storage system.
    ■ **PAUSE POINT** Data can be processed later.

MRI data processing

● **TIMING ~20–32 h.**

▲ **CRITICAL** These times respectively refer to the processing with and without optional GPU acceleration of one MRI dataset on a workstation with similar specifications to the one recommended in this work. For structural MRI processing, the standard FreeSurfer pipeline is considered. Using the FastSurfer tool instead, these computation times can be further reduced by several hours. Processing times for all individual pipelines are given in Table 2.

▲ **CRITICAL** For most processing pipelines of the MRI protocol, GPU processing is optional. Note, however, that for the dMRI pipeline a processing workstation equipped with at least 1 GPU is mandatory. To process a large number of datasets and to speed up the processing time, the use of an HPC cluster is highly recommended, optimally also equipped with GPUs.

18. Convert all MRI data. All DICOM acquisitions must be converted into the NIfTI image file format as the required input format of the image analysis pipelines of the proposed MRI protocol. To this end, for example, the dcmstack converter (https://github.com/moloney/dcmstack) can be used. In the Rhineland Study, compressed NIfTI data are downloaded from XNAT to the HPC resources using the Python library PyXNAT. Alternatively, the curl utility could be used which easily interacts with the RESTful web services provided by XNAT.
    ■ **PAUSE POINT** Data processing can be continued later.
19. Organize all MRI data. Per participant of the imaging study, create a folder with a participant-specific name that stores the NIfTI files of all MR contrasts that should be processed. An example of such a folder structure is provided with the example dataset of this protocol. The proposed MRI protocol does not require data to be stored in the BIDS[66] format. Table 2 provides an overview of which MRI acquisitions are required as input for which processing pipeline. Note that path names for the locations to store the intermediate and final output of the processing pipelines must be given as input when running any pipeline, thus the respective folders must be created as well.
    ▲ **CRITICAL STEP** For a seamless execution of the processing pipelines, avoid subfolders or multiple files of the same MR contrast within the participant data folder. In case of repeated scans for the same MR contrast within one scan session, e.g., due to imaging artifacts or technical issues, the final one needs to be selected as the correct input to the processing pipelines and all others removed from the folder.
    ■ **PAUSE POINT** Data processing can be continued later.
20. Execute analysis pipelines. Executable code to run seven distinct processing pipelines is provided with the proposed MRI protocol and publicly available at https://github.com/orgs/RhinelandStudy/repositories:
    - Pipeline for processing T_1- and T_2-weighted MRI scans using the FreeSurfer recon-all workflow followed by hippocampal subfields segmentation

- Pipeline for white matter hyperintensities segmentation using T_1- and T_2-weighted and FLAIR MRI scans
- Pipeline for olfactory bulb segmentation from T_2-weighted MRI scans
- Pipeline for rs-fMRI data processing
- Pipeline for DSI MRI data processing
- Pipeline for QSM data preprocessing
- Pipeline for adipose tissues segmentation from abdominal MRI (Dixon) scans

▲ **CRITICAL STEP** For each processing pipeline, the README file provides further details on the related literature of the methodology used and the pipeline output folder structure storing the processed imaging data and generated IDPs. The expected input and generated output of each pipeline is presented in Table 2. Every pipeline is executed in the same way. First, depending on the available system for data processing, a Docker or Singularity image must be built or pulled from DockerHub via the Docker or Singularity command provided in the README.md file of each pipeline. Secondly, and in line with the first step, a Docker or Singularity command executes the respective pipeline. The only input arguments required for this command are the path names for the locations to store the intermediate and final output of the processing pipelines and the path name of the MRI data folder that stores all participant folders containing the data to be processed. Running this command with -h will provide additional information on the required and optional function arguments.

◆ **TROUBLESHOOTING**

21. Store processing pipeline outputs. All postprocessed imaging data including the IDPs stored in CSV, JSON or text files are uploaded back to XNAT for permanent archiving using the Python library PyXNAT. Again, for example, the curl utility could be used alternatively.

Troubleshooting

Advice and solutions for troubleshooting potential problems with the MRI protocol can be found in Table 3.

Table 3 | Troubleshooting table

Step	Problem	Possible reason	Solution
2	Imaging artifact is visible in the head scout scan. Acquired MRI data cannot be analyzed	Imaging artifacts in the head scout scan could occur due to tattoos or permanent make-up	Participant should be excluded from the MRI examination
2–11, 15	Participant reports discomfort due to nerve stimulation	Some sequences lead to nerve stimulation in the study participant	These sequences may be skipped
5	Participant had eyes closed during rs-fMRI	Participant fell asleep or forgot to keep the eyes open	Make a note for rs-fMRI data analysis
20	The execution of a pipeline via Docker does not work	Docker is not running on the respective system or the user does not have the permissions to run Docker	If Docker cannot be used, permission to run Singularity also suffices. This container framework is considered safer for HPC systems and converts a Docker image into a Singularity image that can be executed
20	A processing pipeline does not execute and gives the error that a single file (scan name) is required, but a list was provided	Multiple MRI input files of the same contrast are named with similar prefixes in the participant-specific directory	Remove any duplicate MRI input files in the participant-specific directory. See Table 2 for the required pipeline-specific MRI input files
20	CPU code is used instead of the GPU version	GPU is not available or configured with an old Nvidia driver	Please install a compatible Nvidia driver for the GPU
20	Pipeline jobs are killed	Insufficient memory	Make sure sufficient memory is available during the execution of a pipeline

Timing

Steps 1–17: MRI data acquisition ~70 min (Table 1)
Step 18–21: MRI data processing ~20–32 h (Table 2)

Anticipated results

This section presents the outcomes that were obtained by successfully applying the proposed MRI acquisition and processing protocol.

MRI acquisition

Figure 3 shows the unprocessed MRI data collected for one healthy volunteer (male, 34 years old) using the MRI acquisition protocol. The top row shows T_1- and T_2-weighted images (Steps 6 and 7), the FLAIR acquisition (Step 8) and the high-resolution hippocampal subfields imaging data (Step 11). The rs-fMRI data (Step 5) and a $b = 0$ scan without diffusion weighting and diffusion-weighted images for $b = 1{,}000$, 3,000 and 6,000 s/mm^2 (Step 9) are presented in the middle

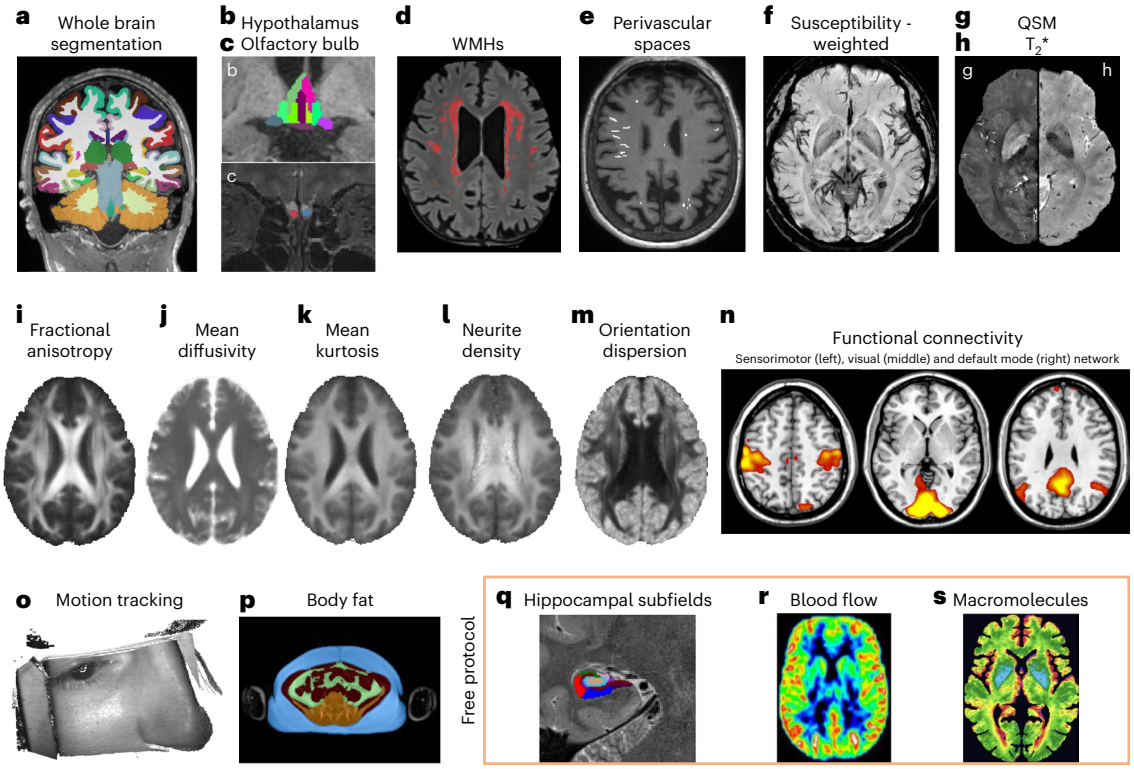

Fig. 4 | Overview of the output of the MRI analysis protocol. a–**e**, Volumetric segmentation of the whole brain (**a**), of regions of interest such as the hypothalamus[42] (**b**) and the olfactory bulb[4] (**c**) and of brain lesions such as WM hyperintensities (**d**) and perivascular spaces (**e**). **f**–**h**, The SWI (**f**) as well as the QSM (**g**) and T_2* map (**h**) obtained from T_2*/susceptibility-weighted MRI. **i**–**m**, Model parameter maps estimated from diffusion-weighted MRI[14] specifically fractional anisotropy (**i**), mean diffusivity (**j**), mean kurtosis (**k**), neurite density (**l**) and orientation dispersion (**m**). **n**, Brain functional connectivity derived using rs-fMRI (sensorimotor (left), visual (middle) and default mode (right) networks). **o**, A rendered raw point cloud generated from depth images acquired using the motion tracking system[11]. **p**, Volumes of subcutaneous and visceral adipose tissue estimated from the abdominal MRI[3]. **q**–**s**, Segmentation of hippocampal subfields (**q**), cerebral blood flow estimated by means of perfusion imaging[67] (**r**) and $T_{1\rho}$ mapping sensitive to macromolecules[20] (**s**). Adapted from ref. 42, CC-BY 4.0 (**b**); ref. 4, CC-BY 4.0 (**c**); ref. 14, CC-BY 4.0 (**i**–**k**, **m**); reproduced from ref. 11, CC-BY 4.0 (**o**); adapted with permission from ref. 3, Wiley (**p**); ref. 67, Elsevier (**r**); ref. 20, International Society for Magnetic Resonance in Medicine (**s**).

row of Fig. 3. The bottom row shows the images obtained through T_2*/susceptibility-weighted (step 10) and body fat (Step 15) imaging. The MRI data used to create the figure are provided as the example dataset of this protocol.

MRI processing

Figure 4 shows an overview of the output that can be obtained from the processing pipelines of the MRI analysis protocol. Brain tissue volume, thickness and surface measures are derived across the whole brain or within regions of interest using multimodal structural MRI: cortical and subcortical structures (Fig. 4a), hypothalamus (Fig. 4b), the olfactory bulb (Fig. 4c) and brain lesions such as WMH (Fig. 4d) and perivascular spaces (Fig. 4e). The SWI (Fig. 4f) as well as the QSM (Fig. 4g) and T_2* map (Fig. 4h) were obtained based on T_2*/susceptibility-weighted MRI. Model parameter maps representing measures of the diffusive molecular transport and the underlying brain tissue microstructure are estimated from diffusion-weighted MRI (Fig. 4i–m). Brain functional connectivity is derived using rs-fMRI (Fig. 4n). A rendered raw point cloud is generated from depth images acquired using the motion tracking system (Fig. 4o). Volumes of subcutaneous and visceral adipose tissue are estimated based on a single-breath-hold abdominal MRI (Fig. 4p). Additionally, the results for three MR contrasts that have also been explored as free protocols in the Rhineland Study are presented: segmentation of hippocampal subfields (Fig. 4q), cerebral blood flow estimated by means of perfusion imaging (Fig. 4r) and $T_{1\rho}$ mapping sensitive to macromolecules (Fig. 4s).

Data availability

The example dataset of one healthy volunteer (male, 34 years old) that includes the MRI acquisitions (Fig. 3) and processing output of most of the pipelines (Fig. 4) using the proposed MRI scan and analysis protocol is publicly available for download from the Zenodo data sharing platform[62] at https://doi.org/10.5281/zenodo.11186582. The Rhineland Study data are not publicly available because of data protection regulations. This includes partly the source data for Fig. 4 and Boxes 2 and 3 in this protocol. However, access can be provided to scientists in accordance with the Rhineland Study's Data Use and Access Policy. Questions regarding data access should be directed to the Rhineland Study Data Use and Access Committee (RS-DUAC@dzne.de).

Code availability

All Rhineland Study MRI sequence protocol parameters are available on GitHub (https://github.com/mrphysics-bonn/mri-protocols/tree/main/rhineland-study). All custom sequence and image reconstruction binaries are provided for various IDEA (Siemens Healthineers) software baselines via Siemens' C2P exchange platform. The provided sequence bundles include the exact Rhineland Study MRI sequence protocol running on the MAGNETOM Prisma scanner (native) and a ported version for less performant Siemens scanners, tested on a MAGNETOM Skyra (compatible). The code for all analysis pipelines is available over the public GitHub code repository and the complete pipelines with the necessary configurations inside the Docker containers, which are also publicly accessible via DockerHub.
The link to the GitHub repository is https://github.com/orgs/RhinelandStudy/repositories where all the pipelines are grouped inside the main repository and the link to the DockerHub registry is docker://dznerheinlandstudie/rheinlandstudie:pipeline_tag where the pipeline tags are named according to their respective GitHub repository name. The SWI, R_2* mapping and QSM pipelines are excluded since they use third-party software not released for sharing. However, the custom preprocessing is included such that afterward any other SWI, R_2* mapping and QSM software can be applied.

Received: 5 January 2024; Accepted: 4 October 2024;
Published online: 13 December 2024

References

1. Brenner, D., Stirnberg, R., Pracht, E. D. & Stöcker, T. Two-dimensional accelerated MP-RAGE imaging with flexible linear reordering. *Magn. Reson. Mater. Phys. Biol. Med.* **27**, 455–462 (2014).
2. Ehses, P., Brenner, D., Stirnberg, R., Pracht, E. D. & Stöcker, T. Whole-brain B_1-mapping using three-dimensional DREAM. *Magn. Reson. Med.* **82**, 924–934 (2019).
3. Estrada, S. et al. FatSegNet: a fully automated deep learning pipeline for adipose tissue segmentation on abdominal dixon MRI. *Magn. Reson. Med.* **83**, 1471–1483 (2020).
4. Estrada, S. et al. Automated olfactory bulb segmentation on high resolutional T_2-weighted MRI. *Neuroimage* **242**, 118464-118464 (2021).
5. Henschel, L. et al. FastSurfer—a fast and accurate deep learning based neuroimaging pipeline. *Neuroimage* **219**, 117012–117012 (2020).
6. Henschel, L., Kügler, D. & Reuter, M. FastSurferVINN: building resolution-independence into deep learning segmentation methods—a solution for HighRes brain MRI. *Neuroimage* **251**, 118933–118933 (2022).
7. Koch, A. et al. Versatile MRI acquisition and processing protocol for population-based neuroimaging. *Alzheimers Dement*. https://doi.org/10.1002/alz.079559 (2023).
8. Lohner, V., Enkirch, S. J., Hattingen, E., Stöcker, T. & Breteler, M. M. B. Safety of tattoos, permanent make-up, and medical implants in population-based 3T magnetic resonance brain imaging: the Rhineland Study. *Front. Neurol.* **13**, 795573 (2022).
9. Lohner, V. et al. Incidental findings on 3T neuroimaging: cross-sectional observations from the population-based Rhineland Study. *Neuroradiology* **64**, 503–512 (2022).
10. Lohner, V. et al. Relation between sex, menopause, and white matter hyperintensities. *Neurology* **99**, e935–e943 (2022).
11. Pollak, C., Kügler, D., Breteler, M. M. B. & Reuter, M. Quantifying MR head motion in the Rhineland Study—a robust method for population cohorts. *Neuroimage* **275**, 120176–120176 (2023).
12. Stirnberg, R. et al. Rapid whole-brain resting-state fMRI at 3T: efficiency-optimized three-dimensional EPI versus repetition time-matched simultaneous-multi-slice EPI. *Neuroimage* **163**, 81–92 (2017).
13. Stirnberg, R. & Stöcker, T. Segmented *K*-space blipped-controlled aliasing in parallel imaging for high spatiotemporal resolution EPI. *Magn. Reson. Med.* **85**, 1540–1551 (2021).
14. Tobisch, A. et al. Compressed sensing diffusion spectrum imaging for accelerated diffusion microstructure MRI in long-term population imaging. *Front. Neurosci.* **12**, 650 (2018).
15. Stirnberg, R., Deistung, A., Reichenbach, J. R., Breteler, M. M. B. & Stöcker, T. Rapid submillimeter QSM and R_2* mapping using interleaved multishot 3D-EPI at 7 and 3 Tesla. *Magn. Reson. Med.* **92**, 2294–2311 (2024).
16. van der Kouwe, A. J. W., Benner, T., Salat, D. H. & Fischl, B. Brain morphometry with multiecho MPRAGE. *Neuroimage* **40**, 559–569 (2008).
17. Breuer, F. A. et al. Controlled aliasing in parallel imaging results in higher acceleration (CAIPIRINHA) for multi-slice imaging. *Magn. Reson. Med.* **53**, 684–691 (2005).
18. Setsompop, K. et al. Blipped-controlled aliasing in parallel imaging for simultaneous multislice echo planar imaging with reduced g-factor penalty. *Magn. Reson. Med.* **67**, 1210–1224 (2012).
19. Bernstein, M. A., Fain, S. B. & Riederer, S. J. Effect of windowing and zero-filled reconstruction of MRI data on spatial resolution and acquisition strategy. *J. Magn. Reson. Imaging* **14**, 270–280 (2001).
20. Kramme, J., Pracht, E. D., Sanroma, G., Stöcker, T. & Breteler, M. M. B. T_1-rho in the aging brain: results from large-scale population imaging. In *Proc. International Society for Magnetic Resonance in Medicine 27*, 2773 (2019).
21. Boland, M. et al. Accelerated 3D-GRASE imaging improves quantitative multiple post labeling delay arterial spin labeling. *Magn. Reson. Med.* **80**, 2475–2484 (2018).
22. Schidlowski, M., Stirnberg, R., Stöcker, T. & Rüber, T. Reliability of quantitative transverse relaxation time mapping with T_2-prepared whole brain pCASL. *Sci. Rep.* **10**, 1–12 (2020).
23. Mueller, S. et al. Whole brain snapshot CEST at 3T using 3D-EPI: aiming for speed, volume, and homogeneity. *Magn. Reson. Med.* **84**, 2469–2483 (2020).
24. Wang, D., Ehses, P., Stöcker, T. & Stirnberg, R. Reproducibility of rapid multi-parameter mapping at 3T and 7T with highly segmented and accelerated 3D-EPI. *Mag. Reson. Med.* **88**, 2217–2232 (2022).
25. Olesen, O. V. et al. Structured light 3D tracking system for measuring motions in PET brain imaging. In *Proc. SPIE 7625, Medical Imaging 2010: Visualization, Image-Guided Procedures, and Modeling* (eds Wong, K. H. & Miga, M. I.) 76250X https://doi.org/10.1117/12.845060 (2010).
26. Olesen, O. V. et al. List-mode PET motion correction using markerless head tracking: proof-of-concept with scans of human subject. *IEEE Trans. Med. Imaging* **32**, 200–209 (2013).
27. Slipsager, J. M. et al. Markerless motion tracking and correction for PET, MRI, and simultaneous PET/MRI. *PLoS ONE* **14**, 1–17 (2019).
28. Kober, T., Marques, J. P., Gruetter, R. & Krueger, G. Head motion detection using FID navigators. *Magn. Reson. Med.* **66**, 135–143 (2011).
29. Marcus, D. S., Olsen, T. R., Ramaratnam, M. & Buckner, R. L. The extensible neuroimaging archive toolkit. *Neuroinformatics* **5**, 11–33 (2007).
30. Gorgolewski, K. et al. Nipype: a flexible, lightweight and extensible neuroimaging data processing framework in Python. *Front. Neuroinform*. https://doi.org/10.3389/fninf.2011.00013 (2011).
31. Friston, K. J. et al. Statistical parametric maps in functional imaging: a general linear approach. *Hum. Brain Mapp.* **2**, 189–210 (1994).
32. Griffanti, L. et al. ICA-based artefact removal and accelerated fMRI acquisition for improved resting state network imaging. *Neuroimage* **95**, 232–247 (2014).
33. Andersson, J. L. R., Skare, S. & Ashburner, J. How to correct susceptibility distortions in spin-echo echo-planar images: application to diffusion tensor imaging. *Neuroimage* **20**, 870–888 (2003).
34. Andersson, J. L. R. & Sotiropoulos, S. N. An integrated approach to correction for off-resonance effects and subject movement in diffusion MR imaging. *Neuroimage* **125**, 1063–1078 (2016).
35. Wedeen, V. J., Hagmann, P., Tseng, W.-Y. I., Reese, T. G. & Weisskoff, R. M. Mapping complex tissue architecture with diffusion spectrum magnetic resonance imaging. *Magn. Reson. Med.* **54**, 1377–1386 (2005).
36. Menzel, M. I. et al. Accelerated diffusion spectrum imaging in the human brain using compressed sensing. *Magn. Reson. Med.* **66**, 1226–1233 (2011).
37. Tobisch, A. et al. Comparison of basis functions and q-space sampling schemes for robust compressed sensing reconstruction accelerating diffusion spectrum imaging. *NMR Biomed.* **32**, 1–15 (2019).
38. Abdul-Rahman, H. S. et al. Fast and robust three-dimensional best path phase unwrapping algorithm. *Appl. Opt.* **46**, 6623–6623 (2007).
39. Schweser, F., Deistung, A., Lehr, B. W. & Reichenbach, J. R. Quantitative imaging of intrinsic magnetic tissue properties using MRI signal phase: an approach to in vivo brain iron metabolism? *Neuroimage* **54**, 2789–2807 (2011).
40. Schweser, F., Sommer, K., Deistung, A. & Reichenbach, J. R. Quantitative susceptibility mapping for investigating subtle susceptibility variations in the human brain. *Neuroimage* **62**, 2083–2100 (2012).
41. Wu, B., Li, W., Guidon, A. & Liu, C. Whole brain susceptibility mapping using compressed sensing. *Magn. Reson. Med.* **67**, 137–147 (2012).
42. Estrada, S. et al. FastSurfer-HypVINN: automated sub-segmentation of the hypothalamus and adjacent structures on high-resolutional brain MRI. *Imaging Neurosci.* **1**, 1–32 (2023).
43. Fischl, B. FreeSurfer. *Neuroimage* **62**, 774–781 (2012).
44. Harms, R. L., Fritz, F. J., Tobisch, A., Goebel, R. & Roebroeck, A. Robust and fast nonlinear optimization of diffusion MRI microstructure models. *Neuroimage* **155**, 82–96 (2017).
45. Fischl, B. et al. Whole brain segmentation: automated labeling of neuroanatomical structures in the human brain. *Neuron* **33**, 341–355 (2002).
46. Faber, J. et al. CerebNet: a fast and reliable deep-learning pipeline for detailed cerebellum sub-segmentation. *Neuroimage* **264**, 119703–119703 (2022).
47. Petersen, M. et al. Reduced olfactory bulb volume accompanies olfactory dysfunction after mild SARS-CoV-2 infection. *Sci. Rep.* **14**, 13396 (2024).
48. Schneider, D. et al. Abdominal fat quantification using convolutional networks. *Eur. Radiol.* https://doi.org/10.1007/s00330-023-09865-w (2023).
49. Wu, T. et al. Automated deep learning–based segmentation of abdominal adipose tissue on dixon MRI in adolescents: a prospective population-based study. *Am. J. Roentgenol.* https://doi.org/10.2214/AJR.23.29570 (2023).
50. Glasser, M. F. et al. The Human Connectome Project's neuroimaging approach. *Nat. Neurosci.* **19**, 1175–1187 (2016).
51. Miller, K. L. et al. Multimodal population brain imaging in the UK Biobank prospective epidemiological study. *Nat. Neurosci.* **19**, 1523–1536 (2016).
52. Jack, C. R. et al. The Alzheimer's disease neuroimaging initiative (ADNI): MRI methods. *J. Magn. Reson. Imaging* **27**, 685–691 (2008).
53. Fox, F. A. U. et al. Association between accelerometer-derived physical activity measurements and brain structure. *Neurology* **99**, E1202–E1215 (2022).
54. Esteban, O. et al. fMRIPrep: a robust preprocessing pipeline for functional MRI. *Nat. Methods* **16**, 111–116 (2019).
55. Schirmer, M. D. et al. White matter hyperintensity quantification in large-scale clinical acute ischemic stroke cohorts—the MRI-GENIE study. *Neuroimage Clin.* **23**, 101884–101884 (2019).
56. Schulze, M. et al. Disentangling early versus late audiovisual integration in adult ADHD: a combined behavioural and resting-state connectivity study. *J. Psychiatry Neurosci.* **46**, 528–537 (2021).
57. Conrad, J. et al. Structural reorganization of the cerebral cortex after vestibulo-cerebellar stroke. *Neuroimage Clin.* **30**, 102603–102603 (2021).
58. Conrad, J. et al. White matter volume loss drives cortical reshaping after thalamic infarcts. *Neuroimage Clin*. https://doi.org/10.1016/j.nicl.2022.102953 (2022).
59. Gajewski, P. D. et al. Impact of biological and lifestyle factors on cognitive aging and work ability in the dortmund vital study: protocol of an interdisciplinary, cross-sectional, and longitudinal study. *JMIR Res. Protoc*. https://doi.org/10.2196/32352 (2022).
60. Claus, J. et al. Physical activity alters functional connectivity of orbitofrontal cortex subdivisions in healthy young adults: a longitudinal fMRI study. *Healthcare* **11**, 689 (2023).

61. Maurer, A. et al. Effects of a 6-month aerobic exercise intervention on mood and amygdala functional plasticity in young untrained subjects. *Int. J. Environ. Res. Public Health* **19**, 6078 (2022).
62. Koch, A. et al. Data from: versatile MRI acquisition and processing protocol for population-based neuroimaging (1.1.0) (dataset). *Zenodo* https://doi.org/10.5281/zenodo.11186582 (2024).
63. Nehrke, K. & Börnert, P. DREAM—a novel approach for robust, ultrafast, multislice B 1 mapping. *Magn. Reson. Med.* **68**, 1517–1526 (2012).
64. Cauley, S. F., Polimeni, J. R., Bhat, H., Wald, L. L. & Setsompop, K. Interslice leakage artifact reduction technique for simultaneous multislice acquisitions. *Magn. Reson. Med.* **72**, 93–102 (2014).
65. Xu, J. et al. Evaluation of slice accelerations using multiband echo planar imaging at 3T. *Neuroimage* **83**, 991–1001 (2013).
66. Gorgolewski, K. J. et al. The brain imaging data structure, a format for organizing and describing outputs of neuroimaging experiments. *Sci. Data* **3**, 160044–160044 (2016).
67. Stöcker, T. in *Advances in Magnetic Resonance Technology and Applications* (eds Choi, I.-Y. & Jezzard, P.) Ch. 1, 3–20 (Academic, 2021).
68. Basser, P. J., Mattiello, J. & LeBihan, D. MR diffusion tensor spectroscopy and imaging. *Biophys. J.* **66**, 259–267 (1994).
69. Jensen, J. H., Helpern, J. A., Ramani, A., Lu, H. & Kaczynski, K. Diffusional kurtosis imaging: the quantification of non-Gaussian water diffusion by means of magnetic resonance imaging. *Magn. Reson. Med.* **53**, 1432–1440 (2005).
70. Zhang, H., Schneider, T., Wheeler-Kingshott, C. A. & Alexander, D. C. NODDI: practical in vivo neurite orientation dispersion and density imaging of the human brain. *Neuroimage* **61**, 1000–1016 (2012).
71. Schaefer, A. et al. Local-global parcellation of the human cerebral cortex from intrinsic functional connectivity MRI. *Cereb. Cortex* **28**, 3095–3114 (2018).
72. Chan, M. Y., Park, D. C., Savalia, N. K., Petersen, S. E. & Wig, G. S. Decreased segregation of brain systems across the healthy adult lifespan. *Proc. Natl Acad. Sci. USA* **111**, E4997–E5006 (2014).
73. Viviani, R. et al. Multimodal MEMPRAGE, FLAIR, and R_2* segmentation to resolve dura and vessels from cortical gray matter. *Front. Neurosci.* **11**, 1–13 (2017).
74. Dietrich, O., Raya, J. G., Reeder, S. B., Reiser, M. F. & Schoenberg, S. O. Measurement of signal-to-noise ratios in MR images: influence of multichannel coils, parallel imaging, and reconstruction filters. *J. Magn. Reson. Imaging* **26**, 375–385 (2007).
75. Friedman, L. & Glover, G. H. Report on a multicenter fMRI quality assurance protocol. *J. Magn. Reson. Imaging* **23**, 827–839 (2006).
76. Jenkinson, M., Beckmann, C. F., Behrens, T. E. J., Woolrich, M. W. & Smith, S. M. FSL. *Neuroimage* **62**, 782–790 (2012).

Acknowledgements

This work was supported by DZNE institutional funds. M.R. was additionally supported by the Federal Ministry of Education and Research of Germany (031L0206, 01GQ1801) and the Chan-Zuckerberg Initiatives Essential Open Source Software for Science RFA (EOSS5 2022-252594). The authors want to thank S. Brunheim for continuous support, i.e., installation, setup, maintenance and documentation of the MRI sequences and protocols in the Rhineland Study, and R. Etteldorf for her support on the deployment of a QA workflow for the FreeSurfer processing pipeline in the Rhineland Study. We also thank all the participants and staff members of the Rhineland Study.

Author contributions

A.K.: methodology, software, validation, data curation, writing–original draft, writing—review and editing, visualization. R.S.: methodology, software, data curation, writing—original draft, writing—review and editing, visualization. S.E.: methodology, software, validation, data curation, writing—review and editing, visualization. W.Z.: methodology, data curation, writing–review and editing, visualization. V.L.: methodology, data curation, writing—review and editing. M.S.: methodology, software, validation, data curation, writing—review and editing. P.E.: methodology, data curation, writing–review and editing. E.D.P.: methodology, data curation, writing—review and editing, visualization. M.R.: conceptualization, methodology, software, validation, supervision, resources, writing—review and editing. T.S.: conceptualization, methodology, software, validation, supervision, resources, writing—review and editing. M.M.B.B.: conceptualization, methodology, validation, supervision, resources, funding acquisition, project administration, writing—review and editing.

Competing interests

The authors declare no competing interests.

Additional information

Correspondence and requests for materials should be addressed to Martin Reuter, Tony Stöcker or Monique M. B. Breteler.

Peer review information *Nature Protocols* thanks Valur Olafsson and the other, anonymous, reviewer(s) for their contribution to the peer review of this process.